Proceedings of the
Annual Stability Conference
Structural Stability Research Council
St. Louis, Missouri, April 16-20, 2013

Shape optimization of cold-formed steel columns with manufacturing constraints and limited number of rollers

J. Leng[1], Z. Li[2], J. K. Guest[3], B. W. Schafer[4]

Abstract
The objective of this paper is to incorporate cold-formed steel manufacturing constraints, i.e., limiting the number of rollers employed for folding the section, in the constrained shape optimization of cold-formed steel columns. The aim of the constrained optimization is the creation of practical and economical cross-sections that provide significant increase in capacity from conventional cross-sections without sacrificing functionality in the field or increasing production costs dramatically. Previously, unconstrained shape optimization of cold-formed steel columns found cross-sections with enormous (as much as 140%) capacity increase above conventional sections, but with overly unconventional shapes. Implementing practical construction constraints in a simulated annealing (SA) algorithm was successful, and resulted in only marginally decreased capacity from the unconstrained optimal solution. The introduction of the manufacturing constraint whereby the number of rollers is limited, is implemented here. The procedure changes the framework of the SA code by making both strip widths and relative turn-angles as design variables for the cross-section stability models implemented in CUFSM. Members with three lengths: 0.61 m [2 ft], 1.22 m [4 ft], and 4.88 m [16 ft], are considered to reflect the impact of different buckling modes (local, distortional, and global) on the optimization results. The number of rollers is varied from 4 to 12 with an increment of 2. Optimized sections from multiple runs show uniformity. Given the larger shape variability provided by having more rollers, optimal designs have a close resemblance to the less constrained results already achieved, such as the point-symmetric 'S'-shaped section for long columns and the singly-symmetric 'Σ'-shaped section for shorter columns. Even with the minimal number of rollers allowed, the average strength increase over an available section is more than fifty percent, which makes the optimized cross-sections promising for developing into new commercial product families.

1. Introduction

[1] Graduate Research Assistant, Dept. of Civil Engineering, Johns Hopkins University, <jleng1@jhu.edu>
[2] Postdoctoral Research Associate, Dept. of Civil Engineering, Johns Hopkins University, <lizhanjie@jhu.edu>
[3] Associate Professor, Dept. of Civil Engineering, Johns Hopkins University, <jkguest@jhu.edu>
[4] Professor and Chair, Dept. of Civil Engineering, Johns Hopkins University, <schafer@jhu.edu>

Cold-formed steel (CFS) has been used extensively in low and midrise buildings, storage racks, car bodies, highway products, transmission towers and other applications as both structural and non-structural members due to its high strength-to-weight ratio and low cost of material and manufacture. Typical CFS thickness is approximately 1 mm [0.04 in.] and typical section depth ranges from approximately 75 to 300 mm [3 to 12 in.]. The member cross-sections are created by bending steel sheets with roll-forming machines. By adjustment of the number and location of rollers, it is possible to form almost any open section. Specifically, many more sections may be produced than the common C- and Z-sections employed in North American commercial practice (e.g. AISI Cold-Formed Steel Design Manual, 2008). Shape optimization of CFS members is a problem of great research value and practical interest.

With low thickness and high slenderness, CFS members are subject to buckling failure, including local plate buckling, distortional buckling, and global (Euler) buckling (Schafer, 2008). Consequently, for CFS members, an optimization problem of importance is to maximize the axial capacity of a column with a given length, coil width (i.e., cross-section perimeter), and sheet thickness.

Previous research explored the unconstrained optimization of CFS members using two types of algorithms: gradient-based and stochastic. The gradient-based search includes deterministic algorithms that depend on exact or approximate forms of first, and/or second-order partial derivatives of the objective function, such as the steepest descent and trust-region methods. The computation of the partial derivatives can be costly, although first order necessary conditions are available for checking convergence. Stochastic search algorithms, like simulated annealing (SA) and genetic algorithms (GA), utilize random perturbations to carry out a wide search of the design space and are potentially able to find global optima without gradient information. However, convergence is probabilistic, and implies multiple replications of the simulation need to be performed to probabilistically locate optima.

The methods utilized to determine nominal axial capacity, P_n, from design specifications also has a great impact on the formulation of the optimization problem. The classical effective width method (AISI-S100-07) is difficult or impossible to be implemented for complicated cross-sections. The Direct Strength Method (DSM, see Appendix 1 of AISI S100-07) only requires the user to provide the critical load in local (P_{crl}), distortional (P_{crd}), and global buckling (P_{cre}), and the load at yield (P_y) for any arbitrary cross-section. This can be coded in a general form amenable to simulation-based optimization. In this work, the author used the finite strip method in the open source software package CUFSM (Schafer et al., 2006 and 2010) to determine P_{crl}, P_{crd}, and P_{cre}.

Previous research on CFS member optimization provides different combinations of strength evaluation criterion from design codes, and optimization algorithms. The classic paper by Seaburg and Salmon (1971) employs the gradient-based steepest descent method to explore the dimensions of hat sections using the effective width method in the AISI Specification (AISI, 1968). Tran and Li (2006) solved the optimization problem of a lipped channel beam using the trust-region method based on various failure modes from the British code BS 5950-5 (British Standard Institution, 1998) and Eurocode (EuroCode-3, 1996). Lu (2003) combined CUFSM with GA to optimize Z-section dimensions largely following the effective width design of

Eurocode 3 (EuroCode-3, 1996). Kolcu et al. (2010) considered Mindlin-Reissner finite strips and used sequential quadratic programming to maximize the critical load P_{cr}. Recently, Chamberlain Pravia and Kripka (2012) used SA to optimize the dimension of a C-section column following the effective width method in the AISI specification. Liu et al. (2004) discussed the use of Bayesian classification trees in CFS member optimization by maximizing P_n with the help of DSM and CUFSM. The authors' previous publication (Leng et al., 2011) showed that several novel cross-sections can be identified as global maximizers of axial capacity P_n using both SA and GA for general search and the steepest descent method for a second search of local optima. Gilbert et al. (2012) proposed 'self-shape optimization' based on floating-point type GA, which is also capable of generating new cross-sections. The application of the algorithm in CFS columns (Gilbert et al., 2012) with CUFSM as the tool for buckling analysis produces optimal cross-sections very close to the authors' existing findings further confirming earlier work.

The work presented here provides the final evolution of practical optimization algorithms for member-level shape optimization of CFS columns. Initially, we formulated our optimization problem as the maximization of axial capacity P_n given a fixed amount of steel sheet. Relative turn-angles of adjacent equal width finite strips were utilized as design variables. Columns with different physical length were studied to reveal the impact of buckling mode on the optimized shapes. The solution provides unconstrained optimal shapes with impressive increase in P_n, but in some cases with no practical potential for production (Leng et al., 2011). Next, constraints based on practical manufacturing and end-use limits were taken into account in the SA algorithm (Leng et al., 2012). An approach is employed in the SA where random perturbations modify the current elite design and check if constraints are satisfied (based on Spall, 2003). The resulting optimal cross-sections include singly-symmetric 'Σ' like sections for short (0.61 m, [2 ft]) and intermediate length (1.22 m, [4 ft]) columns and point symmetric squashed 'S' like sections for long (4.88 m, [16 ft]) columns. All shapes have P_n at least 200% higher than a reference lipped channel 'C' section and all shapes are within at least 10% of the P_n for the unconstrained optimum.

In this work, all manufacturability constraints remain and a limit on the number of rollers (i.e. locations where the section may be folded) is introduced as an additional constraint. This is intended to be regarded as an initial attempt to incorporate the perspective of manufacturing cost into the search process. Technically, this change requires modifying the design variables to enable the change of widths for the finite strips in the CUFSM model. The modified SA code was employed with the allowable number of rollers ranging from 4 to 12 and three physical member lengths (0.61, 1.22 and 4.88 m; [2, 4 and 16 ft]). With only four rollers, the algorithm is essentially the dimension optimization of a lipped channel section (although adjustment in the lip angle is also possible). As the number of rollers increases, greater design freedom is permitted and the optimized shapes bear more resemblance to 'Σ' and squashed 'S' shapes found in constrained optimization with manufacturability constraints only. Even with only four rollers allowed the optimal section P_n is still increased more than 50% from the reference lipped channel section. This research provides a generalized optimization framework to handle constrained optimization of CFS columns and provides cross-sections with great potential in practice and thus can be integrated into system optimization of cold-formed steel buildings.

2. Implement of constraints in simulated annealing algorithm

As discussed previously (Leng et al., 2012), the CFS column cross-section is composed of equal width strip elements in the longitudinal direction and the sheet may be bent at the boundary of the strips. Since the strip width is fixed in advance, only the relative turn-angles between strips are design variables (between $-\pi$ and π, counter clockwise is positive). For example, the lipped channel in Fig. 1(a) is discretized into 42 equal width strips, and only four of the 42 relative turn-angles are non-zero. However, in practical manufacturing using of roll-formers, the number of rollers that can be applied is much smaller, but the distance from roller to roller can vary; therefore, strip width is a natural design variable. The same lipped channel section, now shown in Fig. 1(b), is described by 6 turn-angles and variable lip length, flange width, and web depth. Note, that θ_2, θ_3, θ_5 and θ_6 are the actual locations of the four rollers. Enforcing symmetry, the turn-angle at the mid-point of the web, θ_4, is zero and the cross-section has only three independent strip widths. The values of l_1, l_2 and l_3 are equal to lip length l_l, flange length l_f and half of web length l_w, respectively. For the more complicated singly-symmetric 'Σ'-shaped section of Fig. 1(c) which can be formed using ten rollers, strip 1 and 2 are on the lip and strip 4, 5 and 6 are on the web. As a result, $l_1+l_2=l_l$, $l_3=l_f$, and $l_4+l_5+l_6=l_w$. Since a fixed amount of uniform thickness steel sheet can be represented by the perimeter of the cross-section c, it is natural that $l_l+l_f+l_w=c/2$.

In any given optimization simulation the total number of rollers, n_{rol}, is fixed. Further, we require n_{rol} to be an even number larger than four, since at least four roller rollers are required to create a lipped channel (Fig. 1(a)). With a given n_{rol}, there are $n_{rol}+2$ strips and $n_{rol}+2$ turn-angles. A typical vector of $2n_{rol}+4$ total design variables is given as:

$$\boldsymbol{x} = [l_1, l_2, \cdots l_{n_{rol}+2}, \theta_1, \theta_2, \cdots \theta_{n_{rol}+2}]^T \tag{1}$$

From $\boldsymbol{x}$, the coordinate of every node can be determined. For convenience, the cross-section is generated in the xy plane and the origin of the model is set coincident with the first node. Further, as an end-use constraint the flanges must be parallel with the x axis (Fig. 1). The maximum number of strips on the lip, n_{ml} is determined from n_{rol}. In our formulation, the flange is always flat, and is always treated as one strip. At least one strip must be kept to model one half of the web. Consequently, when $n_{rol}=4$, i.e. only four rollers exist (see Fig. 1(b)), only two strips out of six in total are left for two lips, so n_{ml} must be one. When there are more than four rollers, there can be more strips on the lip. Despite the benefits of complex lips in local and distortional buckling resistance, too many strips on it would increase complexity in forming and leave less design freedom for the optimization of web. As a result, the value of n_{ml} should be within 1 and 3. Note, in analysis using CUFSM, the mesh is doubled, and thus two strips are used to model the flange.

Minimum strip width l_{min}, minimum lip length l_{minl}, minimum flange length l_{minf}, and minimum and maximum web depth (d_{min} and d_{max}) are specified as dimension constraints.

The simulated annealing (SA) algorithm is realized by adding a random perturbation to the design variables of the current elite design in order to create new designs that are then are evaluated against the objective function to compare performance (Arora, 2004). We require the perturbed designs to satisfy all manufacturability constraints. These constraints are fully detailed in previous work (Leng et al., 2012) and illustrated in Fig. 2(a).

The first constraint is that the cross-section must be either symmetric or anti-symmetric, initially set by a randomly generated tag. As a result, this symmetry/anti-symmetry constraint actually creates a mapping that makes only half of total design variables independent. The reduced design vector is:

$$\boldsymbol{x} = [l_1, l_2, \cdots l_{n_{rol}/2+1}, \theta_1, \theta_2, \cdots \theta_{n_{rol}/2+1}]^T \tag{2}$$

Departing from our previous work, we constrained the mid portion of the web to be perpendicular to the flange, and thus turn-angle $\theta_{n_{rol}/2+2}$ is always set as zero. This constraint is required for symmetric cross-sections in our problem: otherwise there would be a fold in the middle of the web and the total number of non-zero turn-angles would be odd. The constraint is not strictly necessary for anti-symmetric cross-sections, but maintained for simplicity. The constraint is also of practical value since a flat area for punching holes is necessary to allow the passage of utilities in typical CFS studs (columns). Assuming the numbers of strips in the lip, the flange and half of the web are $n_l \in \{1, 2, \cdots, n_{ml}\}$, $n_f \equiv 1$ and $n_w = (1 + n_{rol}/2) - n_l - n_f$, then the constraint may be formulated as:

$$\theta_{n_{rol}/2+1} = \begin{cases} -\pi/2, \, if \;\; n_l + 2 = 1 + n_{rol}/2 \\ -\pi/2 - \sum_{i=n_l+2}^{n_{rol}/2} \theta_i, \, otherwise \end{cases} \tag{3}$$

where the condition $n_l + 2 = 1 + n_{rol}/2$ implies one strip to model half of the web.

To ensure the flanges are parallel to the *x* axis the following condition should be satisfied:

$$\theta_{n_l+1} = -\pi - \sum_{i=1}^{n_l} \theta_i \tag{4}$$

Constraint (3) and (4) reduce the number of independent turn-angles to $n_{rol}/2 - 1$. Further, the summation of strip widths should be half of the cross-section perimeter:

$$\sum_{i=1}^{n_{rol}/2+1} l_i = c/2 \tag{5}$$

Thus only $n_{rol}/2$ strip widths can be independently specified.

The second set of constraints contains the preset bounds on cross-section dimensions, including the lower bound on strip width l_i (i is from 1 to n_{rol}+2), flange length l_f, lip length l_l, and the upper and lower bounds on web depth d. Specifically:

$$\begin{cases} l_i \geq l_{min},\ \forall i \in \{1, \cdots, n_{rol}+2\} \\ l_l \geq l_{minl} \\ l_f \geq l_{minf} \\ d_{min} \leq d \leq d_{max} \end{cases} \tag{6}$$

Cross-sections that meet the constraints are randomly generated for the SA routine. First, the number of strips on the lip, n_l, is set by a uniform random integer between 1 and the allowable maximum n_{ml}. Then, the lip length l_l is set by a uniform random number between $\max\{n_l \cdot l_{min}, l_{minl}\}$ and $\left(c - d_{min}\right)/2 - l_{minf}$. Next, the flange length l_f is obtained as a uniform random number between l_{minf} and $\left(c - d_{min}\right)/2 - l_l$. The half of the web length, l_w, that is thus available is $c/2 - l_l - l_f$. Finally, as long as $l_w \geq n_w \cdot l_{min}$, l_l and l_w will be divided into n_l and n_w strip widths respectively. Note, the division is not necessarily uniform: all strips widths are random numbers no less than l_{min}. As shown in Fig. 2(a), the web depth d is the vertical distance between flanges and is less than or equal to the summation of strip widths on the web, $2l_w$. Since d is dependent on the shape of the whole cross-section, its dimension constraint is left as an 'accept or reject' check for the full generated trial cross-section.

Allowance for the passage of utilities is also taken care of in the constraints (Leng et al., 2012). Commercial CFS products (e.g., studs) often have holes punched in the web, leaving space for ducts and piping. An equivalent geometric description is that there should be enough space between the lips (clearance), and any horizontal line in this area cannot intersect with the wall of the cross-section twice to avoid interference (back-folds). The clearance is the shortest vertical distance between any two points on the two lips. A back-fold is a node on the web with a smaller vertical coordinate than the previous node. These constraints are also added as a check of the cross-section, i.e., the clearance should be greater than a specified value, and no back-folds should be detected.

The last constraint has existed since the initial unconstrained optimizations: the cross-section cannot overlap. All unqualified designs are eliminated after a check of self-intersection. Fig. 2(a) is an illustrative cross-section intended to help interpret the manufacturability constraints. The flow-chart in Fig. 3 illustrates the process from initial setup of n_{rol} to the implementation of all constraints. Finally, the mathematical formulation of the constrained maximization of P_n from DSM as an equivalent minimization problem is given by

$$P_n = \min\{P_{ne}, P_{nd}, P_{nl}\} \tag{7}$$

$$\min_{\boldsymbol{x} \in \boldsymbol{X}} \left(f\left(\boldsymbol{x}\right)\right) = \min_{\boldsymbol{x} \in \boldsymbol{X}} \left(-P_n\left(\boldsymbol{x}\right)\right) \tag{8}$$

where $\boldsymbol{X}$ is the feasible set of the mixed design vector of strips widths and turn-angles derived from the above constraints and is difficult to formulate explicitly.

After a design that meets all constraints is generated, CUFSM and DSM are called to evaluate its P_n value, and the main framework of SA starts with the comparison of P_n between the new and

current elite design. It should be pointed out the 'hill-climbing' property of SA makes it possible to accept inferior designs to replace elite ones to expand the search space. This effect is controlled by a parameter called 'temperature'. The probability to accept an inferior design keeps decreasing as the 'temperature' drops geometrically, which finally leads to the convergence of the search to an optimal design. Readers are referred to Leng et al. (2011) for a flow-chart of SA itself in CFS optimization. More theoretical points, variations and applications of SA, etc. are available in the monographs of Arora (2004) and Spall (2003).

In this study, the number of rollers n_{rol} considered is from 4 to 12, with an increment of 2. Dimension constraints l_{min}, l_{minl}, l_{minf}, d_{min} and d_{max} are 6.35, 12.7, 25.4, 92.08 and 228.6 mm [0.25, 0.5, 1.0, 3.625 and 9.0 in.] respectively. The minimum clearance is 25.4 mm [1.0 inch]. The initial design is the same lipped channel cross-section used previously (Leng et al., 2012). This section passes all constraints, with dimensions as shown in Fig. 2(b). The perimeter of the section is 11 in., thickness t = 1 mm [0.04 in.], Young's modulus E = 210000 MPa [30458 ksi], and yielding stress F_y = 228 MPa [33 ksi].

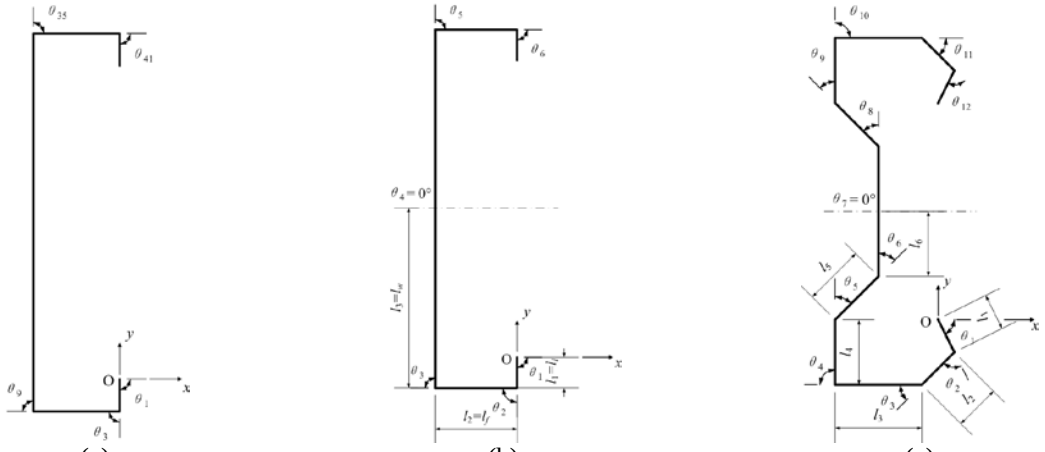

(a) (b) (c)

Figure 1: Comparison of design variables in previous and current research

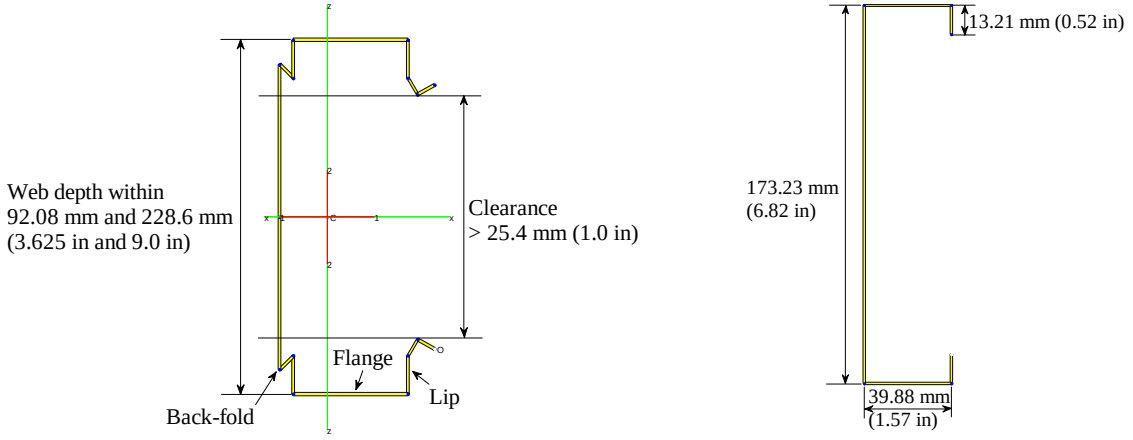

(a) (b)

Figure 2: Illustrations of manufacturability constraints and initial design in optimization

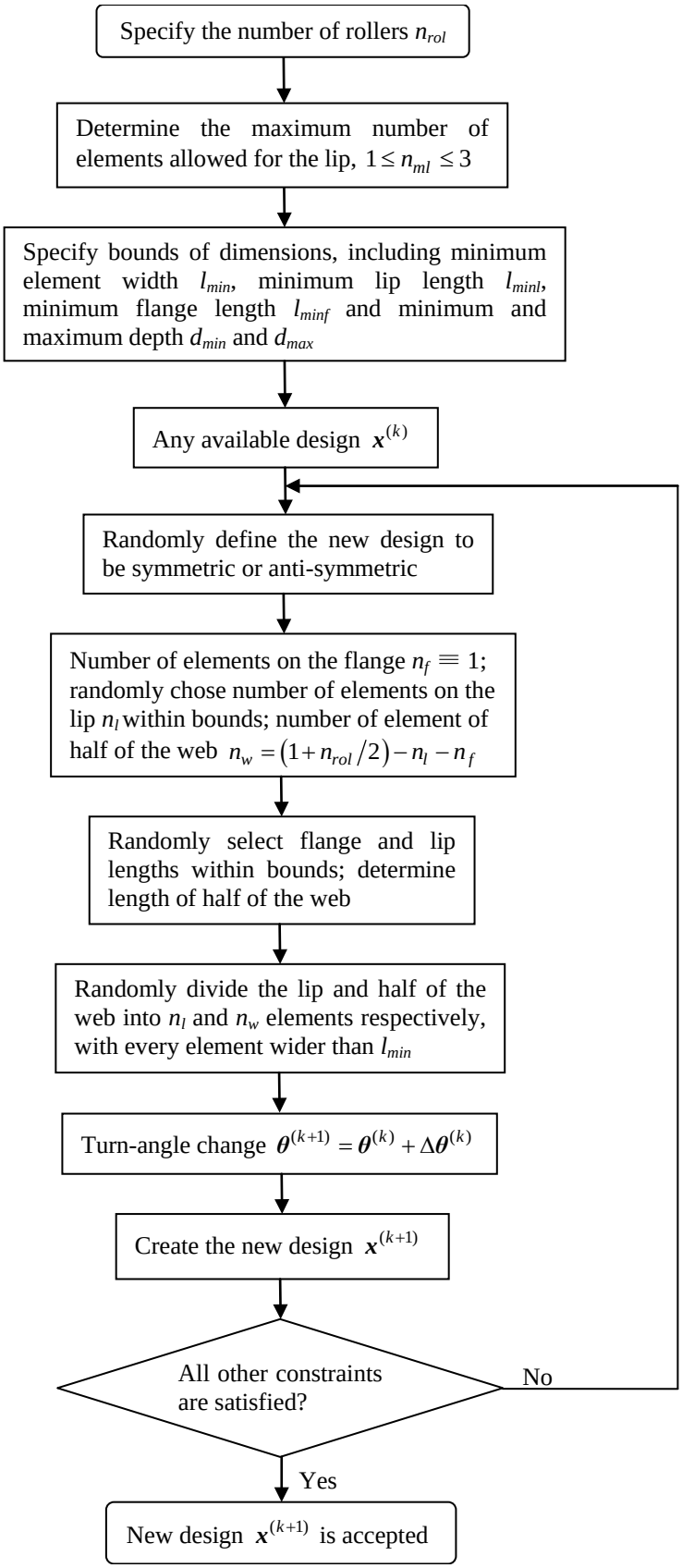

Figure 3: Flow chart of implementation of constraints in simulated annealing algorithm

3. Column optimization result

To illustrate the optimization algorithm and to make a better comparison with previous research findings, columns with three different lengths, 0.61 m [2 ft], 1.22 m [4 ft] and 4.88 m [16 ft] were optimized. The controlling buckling mode generally shifts from local buckling to global buckling as the unbraced length is increased. As discussed above, the number of rollers dictates the dimension of the design space and is therefore another important parameter under investigation.

Controlling parameters of the SA were initiated based on our previous research practice and then fine-tuned. The search begins with an initial temperature $T_0 = 2.0$, and the number of trial designs within one temperature iteration is $k_{max} = 200$. The temperature then drops iteratively with a cooling rate $r = 0.7$, and the maximum number of cooling iterations m_{max}, is 50. At maximum, capacities of 10000 qualified designs are evaluated.

Note, although strip widths and turn-angles are both optimized herein, the dimension of the design space still drops significantly from our previous constrained optimization work and is comparable to our initial unconstrained optimization. A considerable saving of computational resource can be inferred. Although the flange is always regarded as one strip in the shape generation algorithm, the mesh is doubled before calling CUFSM to evaluate critical loads in order to overcome mesh sensitivity.

3.1 Short length (0.61m [2 ft]) column

Starting from the lipped channel section in Fig. 2(b) with the number of rollers ranging from 4 to 12, fifty runs of the SA optimization are performed for 2 ft long columns. For each number of rollers, the three best cross-sections are presented in Fig. 4 to 8 with corresponding nominal capacities listed. One clear observation is that a uniformity of optimized designs has been reached. The optimal shapes are all symmetric, with added complexity in the lips and webs.

When only four rollers are allowed, the algorithm optimizes flange, lip and web dimensions plus an adjustment of the lip angle. It can be inferred that the search of the design space is thorough since all shapes in Fig. 4 have shortened web and lengthened flanges and lips, and the web depth and clearance between the lips are essentially on the constraint boundary, 92.08 mm [3.625 in] and 25.4 mm [1.0 in] respectively.

As more design freedom is enabled by adding the number of rollers, ‘Σ’-like sections manifest themselves as final elite designs. The simplest ‘Σ’ sections are those in Fig. 5 with only one inward stiffener in the middle of the web. A corrugated web and complex lips can be formed, and are formed, when ten or twelve rollers are applied (see Fig. 7 and Fig. 8). As discussed in Schafer et al. (2006), these complex stiffeners are able to provide improved ultimate strength performance over simple stiffeners for relatively short members where the role played by global buckling is trivial. For local buckling, they have shown inward angled stiffeners can: ‘sustain higher buckling loads, as the stiffener provides positive rotational restraint to the attached plate’. Inward angled stiffeners are also conducive to elastic distortional buckling resistance by moving the shear center of the stiffener/flange assembly away from the flange/lip juncture and further away from the flange/web juncture.

Table 1 provides mean and standard deviation of P_n for ten SA optimized shapes with various roller numbers. The small coefficient of variation (about 1%) suggests the algorithm yields highly concentrated optimized results. This concentration may imply a local minimum, but in general SA provides a broad search, and instead implies that the generated optimum is fairly robust. Numerical comparisons between optimized shapes and the original lipped channel 'C' section are given in Table 2. Critical buckling loads and nominal strengths of the three modes of the C-section in Fig. 2(b) and sections in Fig. 4 to 8 are all included. The increase of critical loads for local and distortional buckling contributes directly to the improvement of cross-section capacity. Moreover, there is a considerable amount of capacity increase, even for the simplest case. Fig. 9 depicts the capacity ratio between the mean value of the optimized shapes and the original C-section. A P_n growth of 53% can be achieved by simply modifying strip widths and lip angles of the C-section when only four rollers are available. With eight or more rollers, the optimized 'Σ'–sections have an expected P_n growth increase larger than 120%. Compared with the 'Σ'–sections in the previous constrained optimization with 42 rollers (Leng et al., 2012), the maximum number of rollers considered here is less than one third, but the P_n of the optimized section is 99.7% of previous. This is a great advance since a large growth of column capacity can be realized with little modification of the production line and minimizing the increase in manufacturing cost. A typical convergence curve of the optimization run is presented in Fig. 10. The optimization algorithm found the optimal design after about 3000 objective function evaluations, and the fluctuation illustrates temporal acceptance of inferior designs at the beginning stage of search process. The final optimal design is near the upper bound of axial capacity, the squash load P_y equals 63.70 kN [14.32 kips], and the optimum is only 4.3% less.

Table 1: Mean value and standard deviation of axial capacity P_n of optimized sections of 0.61 m [2 ft] column normalized by P_y = 63.70 kN [14.32 kips]

No. of rollers	4	6	8	10	12
Mean value of P_n/P_y	0.650	0.876	0.946	0.953	0.953
Standard deviation of P_n/P_y	0.001	0.010	0.003	0.001	0.002
Coefficient of variation of P_n	0.002	0.012	0.004	0.001	0.002

Table 2: Critical and nominal loads of C and 'Σ'–sections, normalized by P_y = 63.70 kN [14.32 kips]

Member length (ft.)	Figure	Section	P_{crl}/P_y	P_{crd}/P_y	P_{cre}/P_y	P_{nl}/P_y	P_{nd}/P_y	P_{ne}/P_y	P_n/P_y
2	2b	C	0.162	0.358	4.793	0.424	0.467	0.916	0.424
2	4a	C	0.503	1.505	8.138	0.651	0.869	0.950	0.651
2	5a	'Σ'	1.381	1.642	5.241	0.894	0.893	0.923	0.893
2	6a	'Σ'	2.126	2.087	9.031	0.955	0.950	0.955	0.950
2	7a	'Σ'	2.081	2.939	9.202	0.955	0.998	0.955	0.955
2	8a	'Σ'	1.669	2.264	9.591	0.957	0.966	0.957	0.957
4	2b	C	0.162	0.358	1.282	0.365	0.467	0.721	0.365
4	11a	C	0.503	1.063	2.131	0.592	0.768	0.822	0.592
4	12a	'Σ'	1.284	1.172	1.797	0.786	0.797	0.793	0.786
4	13a	'Σ'	1.448	1.802	2.338	0.836	0.917	0.836	0.836
4	14a	'Σ'	1.531	2.096	2.477	0.845	0.952	0.845	0.845
4	15b	'Σ'	1.557	1.427	2.560	0.849	0.855	0.849	0.849

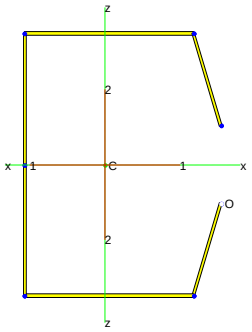

(a) P_n = 41.46 kN [9.32 kips]

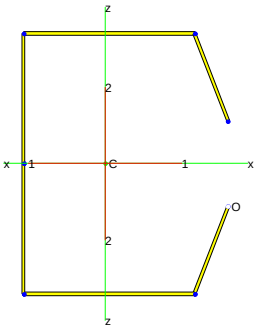

(b) P_n = 41.46 kN [9.32 kips]

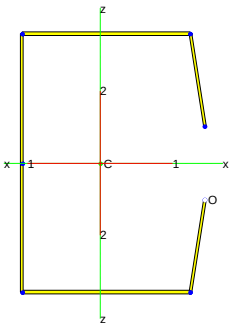

(c) P_n = 41.41 kN [9.31 kips]

Figure 4: Optimal cross-sections found by SA for 0.61 m [2 ft] column, 4 rollers

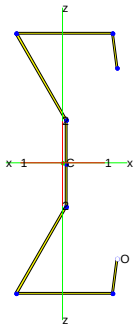

(a) P_n = 56.89 kN [12.79 kips]

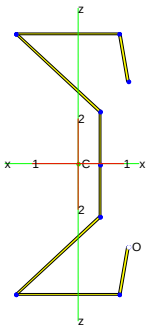

(b) P_n = 56.62 kN [12.73 kips]

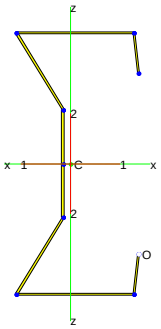

(c) P_n = 56.31 kN [12.66 kips]

Figure 5: Optimal cross-sections found by SA for 0.61 m [2 ft] column, 6 rollers

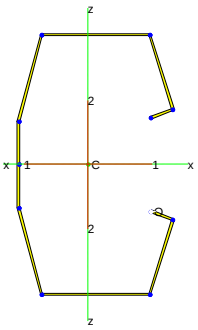

(a) P_n = 60.54 kN [13.61 kips]

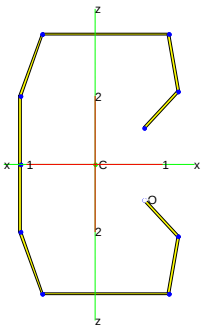

(b) P_n = 60.54 kN [13.61 kips]

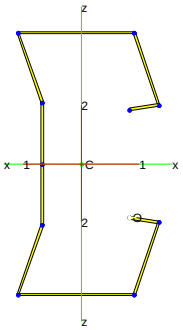

(c) P_n = 60.50 kN [13.60 kips]

Figure 6: Optimal cross-sections found by SA for 0.61 m [2 ft] column, 8 rollers

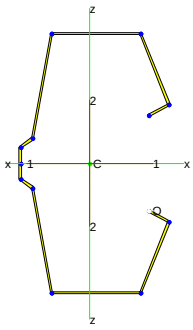

(a) P_n = 60.85 kN [13.68 kips]

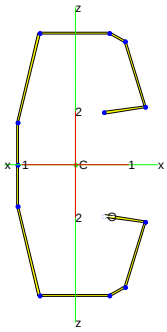

(b) P_n = 60.76kN [13.66 kips]

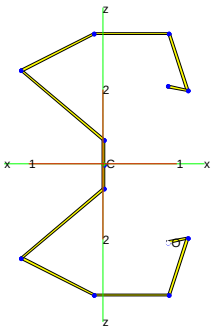

(c) P_n = 60.71 kN [13.65 kips]

Figure 7: Optimal cross-sections found by SA for 0.61 m [2 ft] column, 10 rollers

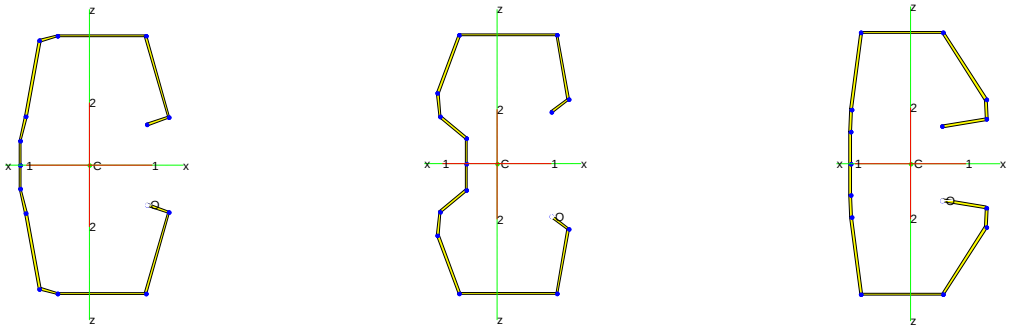

(a) P_n = 60.99 kN [13.71 kips] (b) P_n = 60.81 kN [13.67 kips] (c) P_n = 60.76 kN [13.66 kips]

Figure 8: Optimal cross-sections found by SA for 0.61 m [2 ft] column, 12 rollers

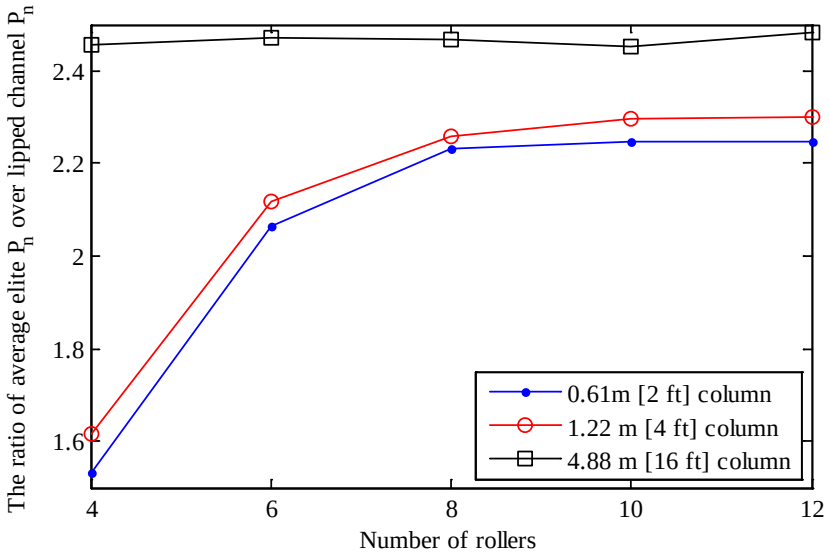

Figure 9: Nominal strength ratio between averages of optimized cross-sections and lipped channel

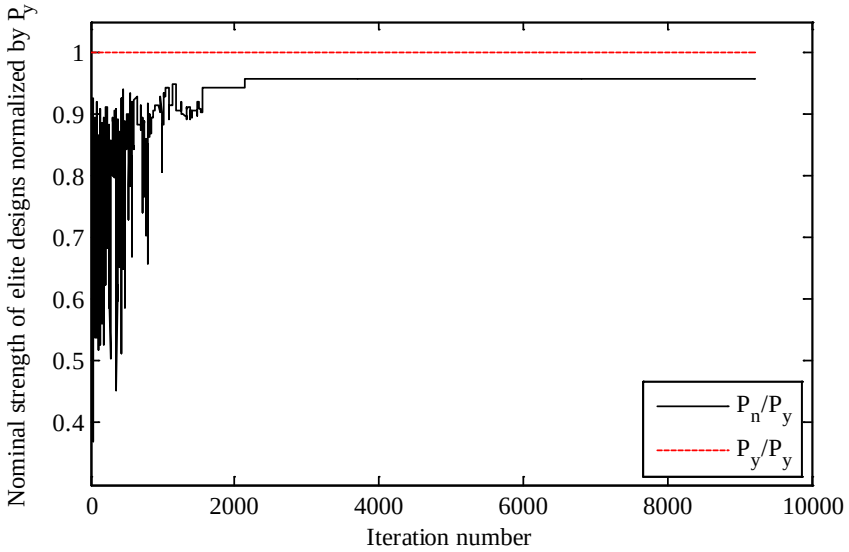

Figure 10: Convergence curve of P_{nelite} for cross-section in Fig. 8 (a)

3.2 Intermediate length (1.22 m [4 ft]) column

Similar to the case of the 0.61 m [2 ft] long columns, SA was run repeatedly for 1.22 m [4 ft] long columns with various numbers of rollers. The top three best designs in terms of P_n are shown in Fig. 11 to Fig. 15 for each roller amount. Optimal cross-sections range from C-sections with short flanges and long lips, as created by 4 rollers, to complex 'Σ'–sections, as created by 12 rollers. For small numbers of rollers (e.g., 4 or 6), the difference between optimal shapes in 0.61 m [2 ft] and 1.22 m [4 ft] columns is negligible. However, for 10 or 12 rollers, the algorithm focused on changes in the lips using up to three rollers (See Fig. 14 and Fig. 15), while for shorter 0.61 m [2 ft] long columns the lip is composed of two flats (two rollers) only and more folds are created in the web (See Fig. 7 and Fig. 8). Again, Schafer's exposition (Schafer et al, 2006) on the effects of complex stiffeners applies. Numerical results of critical loads and axial capacities of related cross-sections are listed in Table 2. Statistical data related to P_n for the optimal sections as listed in Table 3 again serves as an illustration of the uniformity in the SA results.

Cross-sections in Fig. 15 (1.62 m [4 ft], 12 rollers), especially Fig. 15(a), bears a close resemblance to the section found in Fig. 5 of our previous paper on shape optimization of CFS columns (Leng et al., 2012). Both shapes are more regular than the 'Bobby pin' sections found in the unconstrained optimization (Leng et al., 2011). The savings from 42 rollers (unconstrained optimization) to 12 rollers (maximum number explored here) is substantial and only comes at the cost of a trivial strength reduction from 54.49 kN [12.25 kips] to 54.09kN [12.16 kips]. As shown in Fig. 9, the curve of relative P_n with respect to the initial C-section follows the same trend as the short 0.61 m [2 ft] columns, and the percentage of capacity growth is even a little bit higher.

Table 3: Mean value and standard deviation of axial capacity P_n of optimized sections of 1.22 m [4 ft] column, normalized by P_y = 63.70 kN [14.32 kips]

No. of rollers	4	6	8	10	12
Mean value of P_n/P_y	0.589	0.772	0.824	0.838	0.839
Standard deviation of P_n/P_y	0.002	0.010	0.010	0.005	0.006
Coefficient of variation of P_n	0.003	0.013	0.012	0.006	0.007

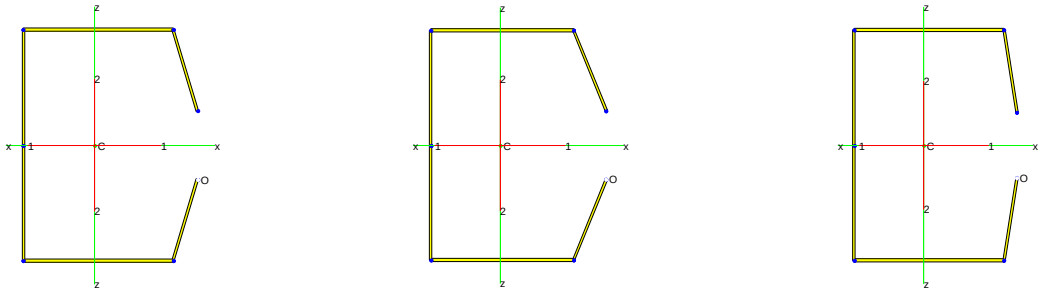

(a) P_n = 37.72 kN [8.48 kips] (b) P_n = 37.63 kN [8.46 kips] (c) P_n = 37.63 kN [8.46 kips]

Figure 11: Optimal cross-sections found by SA for 1.22 m [4 ft] column, 4 rollers

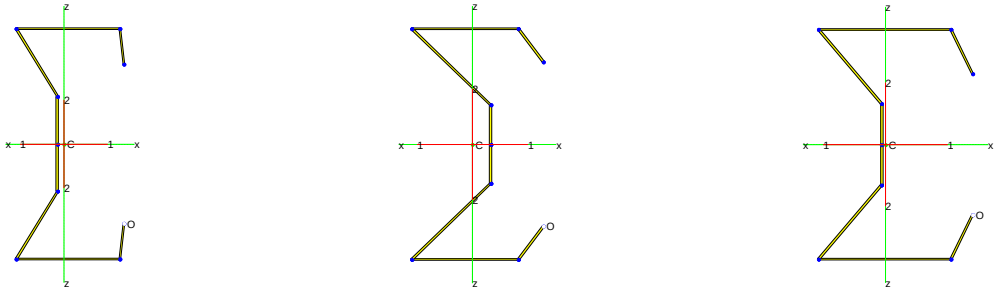

(a) P_n = 50.09 kN [11.26 kips] (b) P_n = 49.78 kN [11.19 kips] (c) P_n = 49.55 kN [11.14 kips]

Figure 12: Optimal cross-sections found by SA for 1.22 m [4 ft] column, 6 rollers

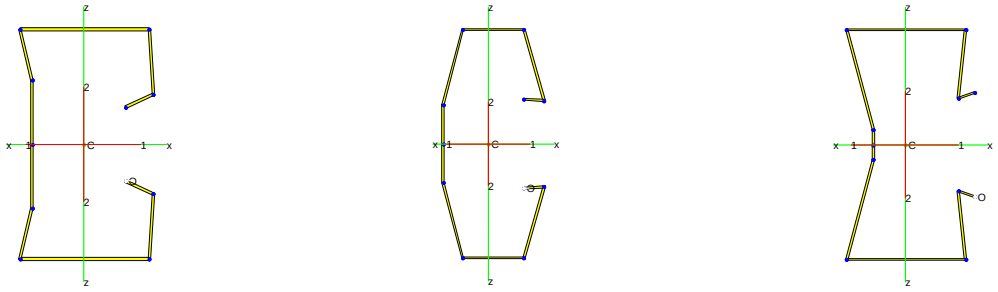

(a) P_n = 53.25 kN [11.97 kips] (b) P_n = 53.11 kN [11.94 kips] (c) P_n = 53.02 kN [11.92 kips]

Figure 13: Optimal cross-sections found by SA for 1.22 m [4 ft] column, 8 rollers

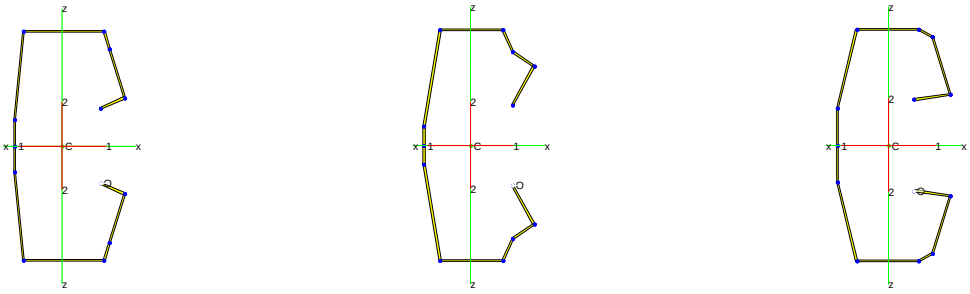

(a) P_n = 53.82 kN [12.10 kips] (b) P_n = 53.69 kN [12.07 kips] (c) P_n = 53.60 kN [12.05 kips]

Figure 14: Optimal cross-sections found by SA for 1.22 m [4 ft] column, 10 rollers

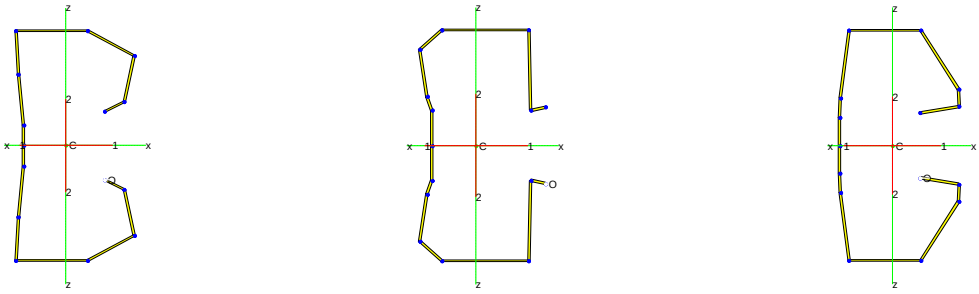

(a) P_n = 54.09 kN [12.16 kips] (b) P_n = 54.05 kN [12.15 kips] (c) P_n = 53.65 kN [12.06 kips]

Figure 15: Optimal cross-sections found by SA for 1.22 m [4 ft] column, 12 rollers

3.3 Long length (4.88 m [16 ft]) column

As shown previously (Leng et al., 2011 and 2012), optimization results for 4.88 m [16 ft] long columns are significantly different from those of 0.61 m [2 ft] and 1.22 m [4 ft] long columns because of the physical nature of global flexural-torsional buckling. The authors discovered that

the anti-symmetric squashed ‘S’ section, featuring a coincidence of the shear center and the centroid, equal moment of inertia about two principal axes, and a large warping coefficient C_w in the unconstrained optimization. Manufacturability constraints fail the equal moment of inertia feature, and P_n of the optimized squashed ‘S’ decreases by less than ten percent from the unconstrained optima.

The same number of algorithm runs (as in the short and intermediate columns) is performed in the optimization of the 4.88 m [16 ft] long columns, but results differ from those shown in past sections. First, the coefficients of variation for P_n of the optimized designs (Table 4), although less than 3%, are uniformly larger than corresponding values in Table 1 and Table 3, indicating the existence of higher diversity in optimization results. Optimized cross-sections in Fig. 16 to Fig. 20, demonstrate a mixture of singly symmetric and anti-symmetric sections, further supporting this argument. When only 4 rollers are allowed, singly symmetric C-sections are still the best option. However, the C-sections (Fig. 16) are characterized by short flanges (near the lower bound) and long, about 45 degree protruding lips, with minimum clearances instead of wide flanges and shortest webs as seen in Fig. 4 and Fig. 11. Anti-symmetric cross-sections with long lips, further derivatives of the squashed ‘S’ sections, start to appear in optimization with 6 rollers and dominate the best shapes when eight or more rollers are allowed.

Table 5 provides the cross-section properties of the optimized shapes. The SA algorithm, with constraints, cannot meet the same global properties as the unconstrained optimal sections. As a result, the axial capacity of the best section (Fig. 18 (a)) is 85.9% of the best squashed ‘S’ section found in the unconstrained optimization. Although this reduction of P_n is non-negligible from an engineer’s perspective, the actual P_n is still 165% greater than the initial C-section in Fig. 2(b), whose P_n is only 4.58 kN [1.03 kips]. On average, one can expect an increase in P_n by more than 140% from the initial C-section even for the cross-section shape optimization with only four rollers involved (see Fig. 9). Unlike short and intermediate columns, the average increase in P_n is not sensitive to the increase in the number of rollers employed. The average performance of the optimized anti-symmetric sections are only modestly better than simple singly-symmetric sections after constraints are introduced, thus the benefits of increasing the number of rollers are limited for long columns.

To understand how the short and intermediate length optimal cross-section would perform at long length the optimal cross-sections in Fig. 4 to Fig. 8 and Fig. 11 to Fig. 15 are considered here as 4.88 m [16 ft] long columns and their axial capacities are evaluated and tabulated in Table 6. Except for the ‘Σ’ sections formed by six rollers, all the other optimized shapes for short and intermediate length columns still perform reasonably well as long columns, rendering an increase of axial capacity of more than 77% from the initial lipped channel C-section of Fig. 2(b). If the number of rollers is eight or greater, the increase is almost 100%, not much lower than the 140% increase yielded from the specially optimized shapes for 4.88 m [16 ft] long columns in Fig. 16 to Fig. 20.

Table 4: Mean value and standard deviation of axial capacity P_n of optimized sections of 4.88 m [16 ft] column, normalized by P_y = 63.70 kN [14.32 kips]

No. of rollers	4	6	8	10	12
Mean value of P_n/P_y	0.177	0.178	0.178	0.177	0.179
Standard deviation of P_n/P_y	0.001	0.002	0.005	0.003	0.004
Coefficient of variation of P_n	0.007	0.012	0.029	0.016	0.023

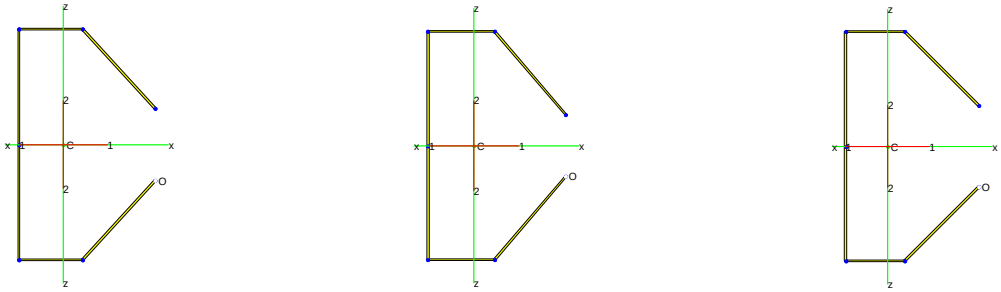

(a) P_n = 11.39 kN [2.56 kips] (b) P_n = 11.39 kN [2.56 kips] (c) P_n = 11.34 kN [2.55 kips]

Figure 16: Optimal cross-sections found by SA for 4.88 m [16 ft] column, 4 rollers

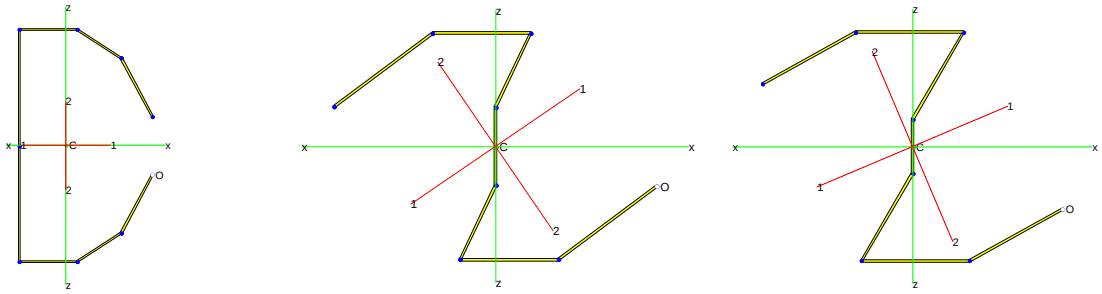

(a) P_n = 11.52 kN [2.59 kips] (b) P_n = 11.48 kN [2.58 kips] (c) P_n = 11.43 kN [2.57 kips]

Figure 17: Optimal cross-sections found by SA for 4.88 m [16 ft] column, 6 rollers

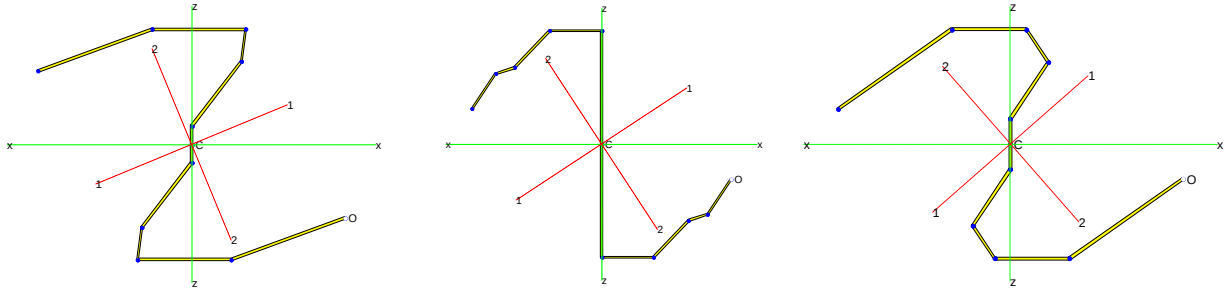

(a) P_n = 12.19 kN [2.74 kips] (b) P_n = 11.43 kN [2.57 kips] (c) P_n = 11.34 kN [2.55 kips]

Figure 18: Optimal cross-sections found by SA for 4.88 m [16 ft] column, 8 rollers

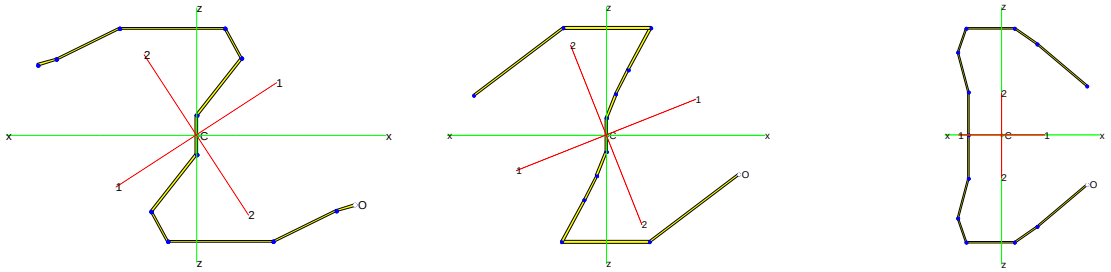

(a) P_n = 11.52 kN [2.59 kips] (b) P_n = 11.39 kN [2.56 kips] (c) P_n = 11.30 kN [2.54 kips]

Figure 19: Optimal cross-sections found by SA for 4.88 m [16 ft] column, 10 rollers

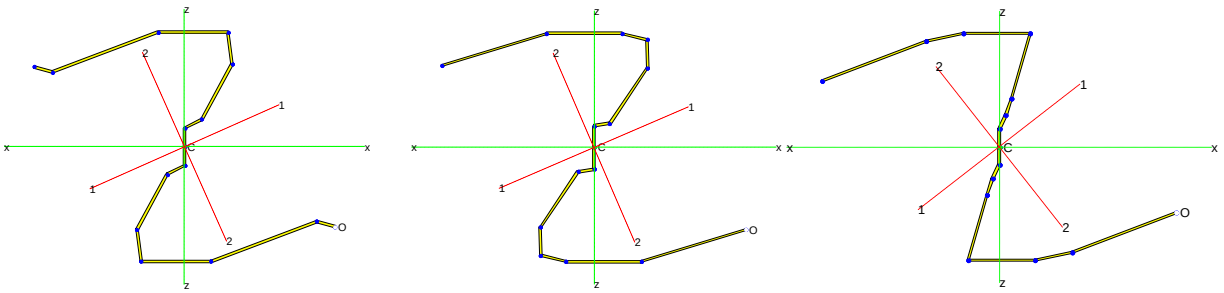

(a) P_n = 11.92 kN [2.68 kips] (b) P_n = 11.65 kN [2.62 kips] (c) P_n = 11.43 kN [2.57 kips]

Figure 20: Optimal cross-sections found by SA for 4.88 m [16 ft] column, 12 rollers

Table 5: cross-section properties of optimized sections of 4.88 m [16 ft] member

Section	Figure	I_{11} (cm^4)	I_{22} (cm^4)	C_w (cm^6)	$\sqrt{x_0^2 + y_0^2}$ (cm)	P_n (kN)
C	16a	47.16	14.94	863.07	5.37	11.39
C	17a	45.95	15.07	913.83	5.46	11.52
Squashed 'S'	18a	41.62	15.86	557.21	0	12.19
Squashed 'S'	19a	49.53	15.03	653.62	0	11.52
Squashed 'S'	20a	42.25	15.57	583.80	0	11.92

Table 6: Axial capacities of optimal cross-sections of 0.61 m [2 ft] and 1.22 m [4 ft] members evaluated as 4.88 m [16 ft] member

Member length (ft)	Figure	Section	P_n (kN)	Member length (ft)	Figure	Section	P_n (kN)
2	4a	C	8.14	4	11a	C	8.14
2	5a	'Σ'	4.85	4	12a	'Σ'	6.41
2	6a	'Σ'	9.03	4	13a	'Σ'	9.07
2	7a	'Σ'	9.30	4	14a	'Σ'	8.94
2	8a	'Σ'	9.56	4	15b	'Σ'	9.25

4. Discussion and future works

The authors have proposed that gradient based algorithms, like steepest descent method, and stochastic gradient algorithms, like simultaneous perturbation stochastic approximation, can be used as local optimizers to modify stochastic search results. The idea is laid aside in optimization with a limited number of rollers since the problem considered herein is fairly close to the real world manufacturing of commercial products and the cross-sections found by SA in previous sections can be fabricated using current facilities with minimal difficulty. Thus, our shape optimization work of CFS columns, starting from tests of algorithm usefulness and unconstrained optimization to find sections that maximize P_n, finally turns out to be a code that can provide cross-sections of practical value with a credible amount of capacity increase – more than 100% from conventional lipped channels as long as eight rollers are applied.

An active extension of this current work is to systematically generate a family of cross-sections (like those in the SSMA inventory, SSMA, 2011), but with improved capacity and material efficiency. Fig. 4 shows that when the number of rollers reaches six, our shape optimization algorithm can develop cross-sections that double axial capacity P_n for short, intermediate and long columns respectively. Although long column optimization with global buckling poses some unique requirements on the section shape, optimal shapes for local and distortional buckling

controlled cases still perform reasonably well to resist global buckling. Consequently, it is possible to design cross-sections that have relatively large buckling strength for all buckling modes and still meet reasonable manufacturing and construction constraints. Such optimized cross-sections can form a family of potential sections with a much smaller variation in dimensions and number of rollers, so that production cost can be further reduced.

5. Conclusion

A series of construction and manufacturing constraints, together with limits on number of rollstands where the section may be folded (i.e. the number of rollers) ranging from 4 to 12, is implemented in simulated annealing code for cross-section shape optimization of cold-formed steel columns. Both flat widths and relative turn-angles between strips are design variables in the stochastic search seeking sections that maximize the nominal axial strength P_n evaluated using the Direct Strength Method and finite strip (CUFSM) simulation results for critical buckling loads.

Columns with short 0.61 m [2 ft], intermediate 1.22 m [4 ft], and long 4.88 m [16 ft] physical lengths were studied. Fifty SA-based optimization simulations were run in each case and the three best optimal cross-sections were selected for every combination of number of rollers and member length. Statistics of P_n and plots of the optimal sections illustrate the uniformity of the stochastic search results for any of these combinations. A considerable increase of P_n is always available from the optimization, demonstrating the power of the algorithm. Singly-symmetric sections are always optimal designs for short and intermediate unbraced length columns. For four rollers (four folds), only C-sections with shallow webs, long flanges and lips can be formed, but P_n is still optimized to a more than 50% above the initial C-section. For larger numbers of rollers (folds) ‘Σ’-sections can be formed providing a further increase of P_n up to more than 100%. For long columns, optimization with 4 rollers yields a C-section with short flanges and long protruding lips. Squashed ‘S’ sections, found by the authors in past research, starts to appear in long columns when more rollers (folds) are allowed. Numerical comparison indicates that the anti-symmetric squashed ‘S’ sections which meet the construction and manufacturing constraints largely lose their superiority over singly-symmetric sections (In unconstrained optimization anti-symmetric sections were clearly superiors). For long columns the optimal solutions all provide at least a 140% increase over the reference (initial) C-section.

Compared with previous work of the authors the formulation based on a finite number of folds (rollers) lead to a reduced dimension of the design space and the total number of objective function evaluations and the machine time for each CUFSM analysis both decreased. The optimal shapes that meet the construction and manufacturing constraints have significant potential for commercial application. Of the optimal sections explored the ‘Σ’-sections developed here are currently preferred due to their ability to provide robust capacity increases across all studied limit states/unbraced lengths, yet require only minimal change in current manufacturing and construction.

Acknowledgments

This project received partial funding from U.S. National Science Foundation project: NSF-OISE-1103894: US Egypt Cooperative Research: Use of Cold-Formed Steel in Residential Housing. Any opinions, findings, and conclusions or recommendations expressed in this publication are

those of the author(s) and do not necessarily reflect the views of the National Science Foundation.

References

American Iron and Steel Institute. (1968). 'AISI specification for the design of cold-formed steel structural members.' Washington, DC: American Iron and Steel Institute.

American Iron and Steel Institute. (2007). 'North american specification for the design of cold-formed steel structural members (AISI S100-2007 ed.).' Washington, DC: American Iron and Steel Institute.

American Iron and Steel Institute. (2008). 'Cold-formed steel design manual (D100-08 ed.).' Washington, DC: American Iron and Steel Institute.

Arora, J. S. (2004). 'Introduction to optimum design (2nd ed.).' Academic Press.

British Standard Institution. (1998). 'Structural use of steel in building: Part 5: Code of practice for design of cold formed sections (BS5950 ed.).' British Standard Institution.

Chamberlain Pravia, Z. M., & Kripka, M. (2012). 'Cross section optimization using simulated annealing of cold-formed steel channel columns.' *Proceedings of the Annual Stability Conference Structural Stability Research Council*, Grapevine, TX.

EuroCode-3. (1996). 'Design of steel structures, part1.3: General rules for cold formed thin gauge members and sheeting.' British Standard Institution.

Gilbert, B. P., Savoyat, T. J. M., & Teh, L. H. (2012). 'Self-shape optimisation application: Optimisation of cold-formed steel columns.' *Thin-Walled Structures*, 60, 173-184.

Gilbert, B. P., Teh, L. H., & Guan, H. (2012). 'Self-shape optimisation principles: Optimisation of section capacity for thin-walled profiles.' *Thin-Walled Structures*, 60, 194-204.

Kolcu, F., Ekmekyapar, T., & Özakça, M. (2010). 'Linear buckling optimization and post-buckling behavior of optimized cold formed steel members.' *Scientific Research and Essays*, 5(14), 1916-1924.

Leng, J., Guest, J. K., & Schafer, B. W. (2011). 'Shape optimization of cold-formed steel columns.' *Thin-Walled Structures*, 49(12), 1492-1503.

Leng, J., Li, Z., Guest, J. K., & Schafer, B. W. (2012). 'Constrained shape optimization of cold-formed steel columns.' *Proceedings of Twenty-First International Specialty Conference on Cold-Formed Steel Structures* , St. Louis, MO. 59-73

Li, Z., & Schafer, B. W. (2010). 'Application of the finite strip method in cold-formed steel member design.' *Journal of Constructional Steel Research*, 66(8), 971-980.

Liu, H., Igusa, T., & Schafer, B. (2004). 'Knowledge-based global optimization of cold-formed steel columns.' *Thin-Walled Structures*, 42(6), 785-801.

Lu, W. (2003). 'Optimum design of cold-formed steel purlins using genetic algorithms.' Helsinki University of Technology.

Schafer, B. W. (2008). 'Review: The direct strength method of cold-formed steel member design.' *Journal of Constructional Steel Research*, 64(7), 766-778.

Schafer, B. W. (2010). 'User's manual and tutorials of CUFSM 3.12.' Johns Hopkins University. http://www.ce.jhu.edu/bschafer/cufsm/cufsm312/index.htm

Schafer, B. W., & Ádány, S. (2006). 'Buckling analysis of cold-formed steel members using CUFSM: Conventional and constrained finite strip methods.' *Proceedings of Eighteenth International Specialty Conference on Cold-Formed Steel Structures*, Orlando, FL. 39-54.

Schafer, B. W., Sarawit, A., & Peköz, T. (2006). 'Complex edge stiffeners for thin-walled members.' *Journal of Structural Engineering*, 132(2), 212-226.

Seaburg, P. A., & Salmon, C. G. (1971). Minimum weight design of light gage steel members. *Journal of the Structural Division*, 97(1), 203-222.

Spall, J. C. (2003). 'Introduction to stochastic search and optimization: Estimation, simulation, and control.' Hoboken, NJ: John Wiley and Sons.

Steel Stud Manufacturers Association. (2011). 'Product technical information complies with 2009 IBC SSMA.' http://www.ssma.com

Tran, T., & Li, L. (2006). 'Global optimization of cold-formed steel channel sections.' *Thin-Walled Structures*, 44(4), 399-406.